Nanomimics of Host Cell Membranes Block Invasion and Expose Invasive Malaria Parasites

Adrian Najer,[†,‡,§] Dalin Wu,[†] Andrej Bieri,[#] Françoise Brand,[‡,§] Cornelia G. Palivan,[†] Hans-Peter Beck,[‡,§] and Wolfgang Meier*[,†]

[†]Department of Chemistry, University of Basel, Klingelbergstrasse 80, CH-4056 Basel, Switzerland, [‡]Swiss Tropical and Public Health Institute, Socinstrasse 57 Postfach, CH-4002 Basel, Switzerland, [§]University of Basel, Petersgraben 2, CH-4002 Basel, Switzerland, and [#]Center for Cellular Imaging and Nano Analytics, Biozentrum, University of Basel, Mattenstrasse 26, CH-4058 Basel, Switzerland

ABSTRACT The fight against most infectious diseases, including malaria, is often hampered by the emergence of drug resistance and lack or limited efficacies of vaccines. Therefore, new drugs, vaccines, or other strategies to control these diseases are needed. Here, we present an innovative nanotechnological strategy in which the nanostructure itself represents the active substance with no necessity to release compounds to attain therapeutic effect and which might act in a drug- and vaccine-like dual function. Invasion of *Plasmodium falciparum* parasites into red blood cells was selected as a biological model for the initial validation of this approach. Stable nanomimics—polymersomes presenting receptors required for parasite attachment to host cells—were designed to efficiently interrupt the life cycle of the parasite by inhibiting invasion. A simple way to build nanomimics without postformation modifications was established. First, a block copolymer of the receptor with a hydrophobic polymer was synthesized and then mixed with a polymersome-forming block copolymer. The resulting nanomimics bound parasite-derived ligands involved in the initial attachment to host cells and they efficiently blocked reinvasion of malaria parasites after their egress from host cells *in vitro*. They exhibited efficacies of more than 2 orders of magnitude higher than the soluble form of the receptor, which can be explained by multivalent interactions of several receptors on one nanomimic with multiple ligands on the infective parasite. In the future, our strategy might offer interesting treatment options for severe malaria or a way to modulate the immune response.

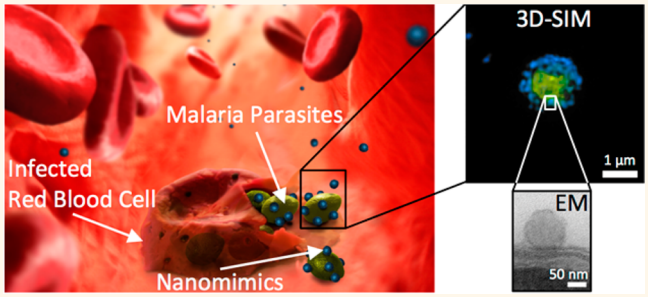

KEYWORDS: block copolymer · vesicle · polymersome · self-assembly · nanomedicine · infectious disease · *Plasmodium*

Infectious diseases—causing about 25% of total annual deaths worldwide—are a major threat to public health, which is enhanced by the emergence of drug resistance and vaccine failures.[1,2] In the case of malaria, there is no vaccine registered yet, and drug susceptibility is decreasing; resistance to artemisinin derivatives, which in combination with other drugs are the recommended first-line treatments, is already spreading across mainland Southeast Asia.[3] An emerging strategy for fighting infectious diseases is to inhibit the initial host–pathogen interaction,[4,5] thus preventing cell invasion as presented here in the case of malaria. A large number of human pathogens use the cell surface heparan sulfate proteoglycan for recognition and primary interaction between host and pathogen.[6] *Plasmodium falciparum*, which causes malaria and is responsible for >600 000 deaths annually,[7] uses heparan sulfate as the receptor for initial binding of sporozoites to hepatocytes[8] and merozoites to host red blood cells (RBCs).[9] Highly sulfated polysaccharides such as heparin (closely related to heparan sulfate) or K5 polysaccharide are potent inhibitors of merozoite invasion of RBCs *in vitro*. Although different strains of *P. falciparum* use different pathways for RBC invasion, six different parasite strains were tested and were inhibited by these sugars.[9] It has been shown that soluble heparin *in vitro* and *in vivo* can also reverse binding required for sequestration and rosetting in *P. falciparum* infections, which are the major pathogenic events.[10,11] However, the use of these polysaccharides in malaria infections

* Address correspondence to wolfgang.meier@unibas.ch.

Received for review September 24, 2014 and accepted November 29, 2014.

Published online November 29, 2014
10.1021/nn5054206

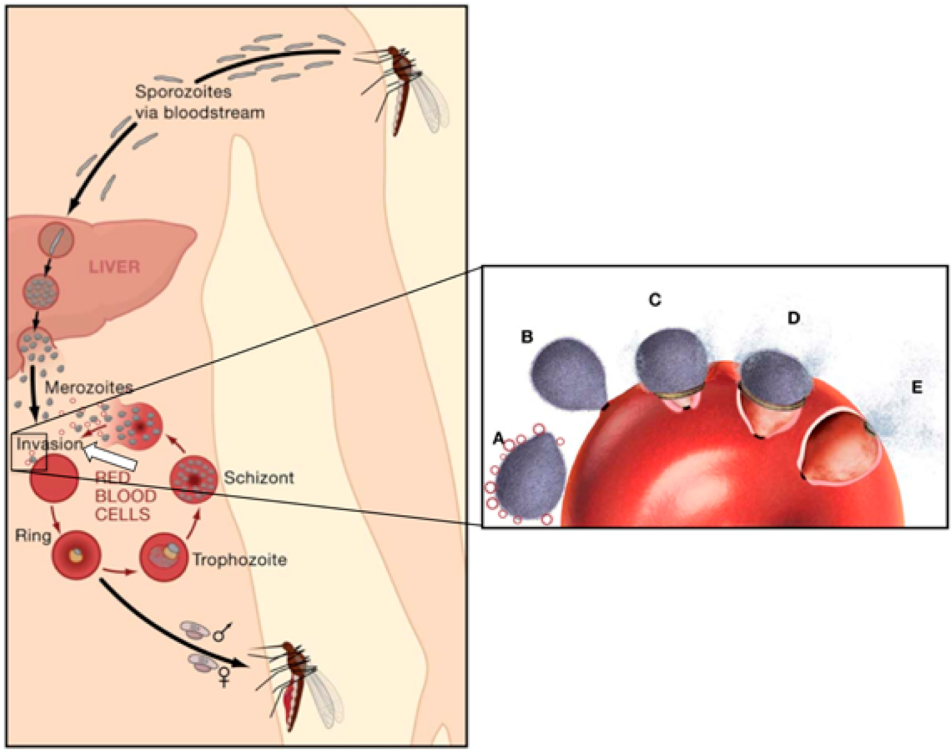

Scheme 1. Schematic presentation of the nanomimic concept. (Left) Life cycle of *P. falciparum* in the human host: an *Anopheles* mosquito injects sporozoites, which pass through Kupffer cells and invade hepatocytes, in which merozoites develop and are released into the bloodstream to invade red blood cells (RBCs) after specific attachment to heparan sulfate.[9] In infected RBCs (iRBCs) merozoites develop through schizogeny, releasing 16−32 daughter merozoites after 48 h, which subsequently invade new RBCs (asexual blood stage). (Right) Schematic merozoite invasion into RBCs. (A) Initial attachment through binding of the processed ligand $MSP1_{42}$ to heparan sulfate on RBCs.[9] Competing nanomimics (red circles) block fresh merozoites before they enter new RBCs (white arrow) (modified with permission from ref 32).

is hindered by short *in vivo* circulation half-lives (about 30 min to 2 h),[12,13] limited efficacy, and anticoagulation properties, which led to intracranial bleedings (in the case of heparin).[11,14] Naturally acquired immunity to malaria is largely directed against extracellular merozoites[15] and protects semi-immune individuals from developing severe forms of the disease. Yet, there is no drug that targets the process of invasion of erythrocytes,[16] although some candidates are known.[17] The recent advent of whole attenuated parasite vaccines is accompanied by concerns about production, distribution, and safety,[18] while the limited protection obtained after vaccination with subunit vaccines[19,20] emphasizes the need for alternative treatment and vaccination strategies.

Nanotechnology provides promising tools for designing innovative structures that could be used to combat complex infections,[21−23] but as yet has been applied only sparsely to malaria and was focused on systems for drug or vaccine delivery.[24] With other pathogens, mainly bacteria and viruses, few lipid-based nanostructures have been evaluated for inhibition of host−pathogen interactions.[5] However, liposomes, which are the most simple membranous nanostructures that ensure lateral mobility of receptors for multivalent ligand interaction, possess poor stability and structural integrity *in vivo*.[5] Polymer-based vesicles (polymersomes) composed of amphiphilic block copolymers represent an alternative 3D membranous structure for host cell membrane-nanomimics to interact with or to neutralize pathogens in the bloodstream. They have the advantage of a biomimetic membrane structure, a higher stability than liposomes,[25] and long *in vivo* circulation times.[26] Polymersomes have been extensively studied as carriers for active compounds ranging from low molecular mass drugs to proteins and nucleic acids, and they can compartmentalize *in situ* reactions, resulting in the development of nanoreactors and artificial organelles.[27] So far, polymersomes have been designed to present viral receptors on their surface for virus-assisted loading of polymersomes[28] or to study viral protein binding.[29] In addition, heparin has been used at the surface of solid nanoparticles to achieve long circulation times in the bloodstream for drug delivery in cancer therapy.[30,31]

Here, we introduce nanomimics based on polymersomes that present attachment receptors and thus mimic RBC membranes as a nanotechnological strategy for blocking invasion (drug action) and increased exposure of the infective form of *P. falciparum* to the immune system (vaccine-like action) (Scheme 1).

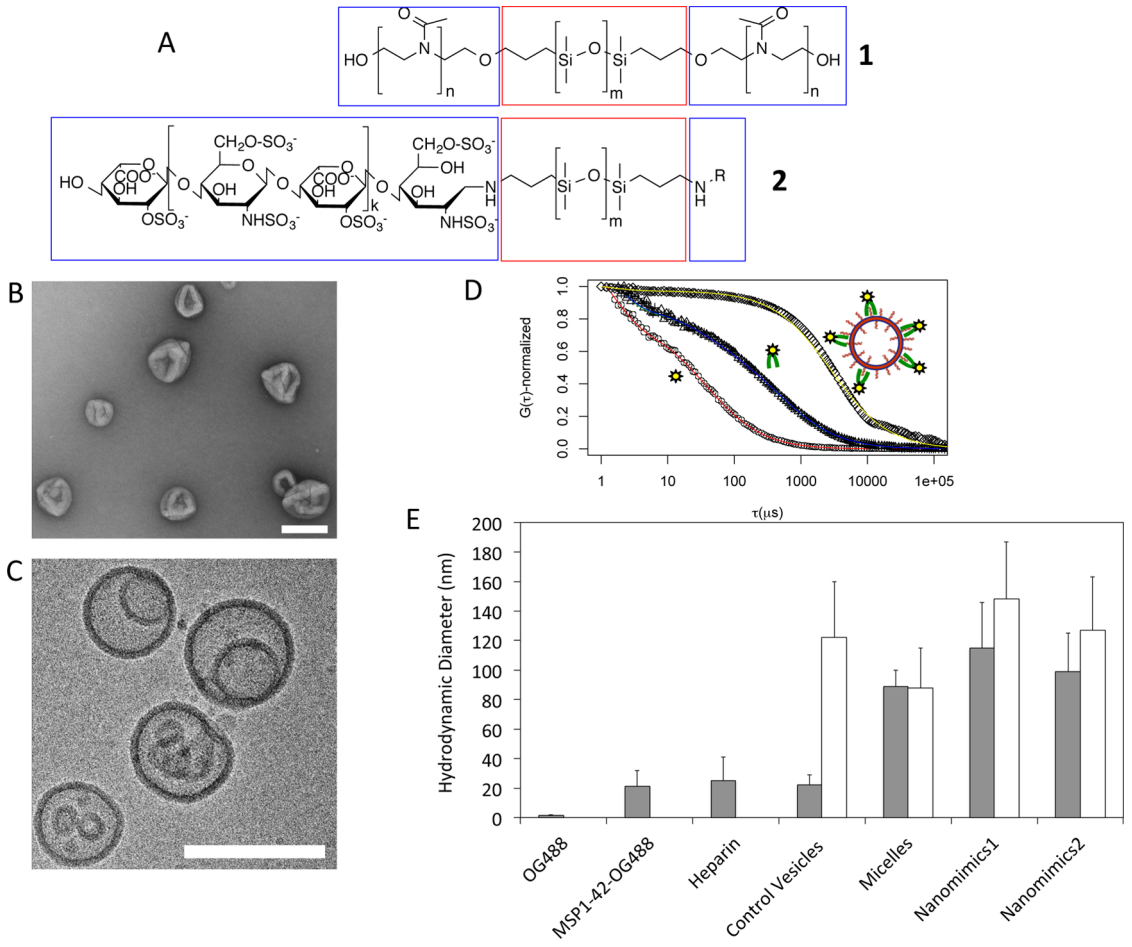

Figure 1. Characteristics of nanomimics. (A) Chemical structure of PMOXA-*b*-PDMS-*b*-PMOXA (1) and PDMS-heparin (2). R is either a proton or another heparin chain. (B) TEM image of nanomimics. (C) Cryo-TEM of the same nanomimics. Scale bars: 200 nm. (D) Normalized autocorrelation curves from FCS data in PBS: free OG488 (red), free *Pf*MSP1$_{42}$-OG488 (blue), control polymersomes with *Pf*MSP1$_{42}$-OG488 (green), and nanomimics with *Pf*MSP1$_{42}$-OG488 (yellow). (E) Hydrodynamic diameters (D_H) obtained from mixtures of *Pf*MSP1$_{42}$-OG488 with controls (free heparin or control polymersomes) and nanomimics (gray bars). Data from dynamic light scattering are included for the nanostructures for comparison (white bars). Only when heparin was present on the surface of nanostructures (micelles, nanomimics) and mixed with *Pf*MSP1$_{42}$-OG488 did the diffusion time shift to the corresponding nanostructure size, indicating that *Pf*MSP1$_{42}$-OG488 bound to the nanostructures. Mixtures with free heparin or control polymersomes yielded no difference from free *Pf*MSP1$_{42}$-OG488 diffusion (errors are ±standard deviation).

Nanomimics were built by self-assembly of a mixture of a polymersome-forming block copolymer with a copolymer based on a hydrophobic block and the host cell receptor as hydrophilic domain. We used *Plasmodium* merozoites as a model to exemplify the concept of efficient blockage of pathogen reinvasion after egress from their host cells *in vitro*. The intrinsic 3D architecture of nanomimics combined with the specificity of heparin selected as receptor represents an essential step to gain efficacy by exposing multiple receptors on one nanomimic, which serve to block the parasite in a multivalent binding fashion. Due to the use of this key receptor of host cell membranes, it is expected to open efficient directions in addressing other infections that rely on the same receptor and have a similar way of reproduction.

RESULTS AND DISCUSSION

Block Copolymer Synthesis. Heparan sulfate has been shown to play a critical role as a receptor for the initial attachment of merozoites to RBCs;[9,33] therefore we selected the closely related heparin, which is a potent inhibitor of merozoite invasion of RBCs *in vitro*,[9] for exposure on the exterior surface of nanomimics. Heparin is commercially readily available and has a closely related chemical structure to other sugar chains that have been reported as bioactive without anticoagulation property (*e.g.*, K5 polysaccharide).[9] We prefer heparin as a receptor model to be exposed on nanomimics, as it is a very well-known macromolecule, which serves as a straightforward proof of concept; related polysaccharides such as K5 or nonanticoagulant heparin will be then used for the optimization of nanomimics.

To produce model nanomimics, two different block copolymers were synthesized. The biocompatible, polymersome-forming ABA block copolymer poly(2-methyl-2-oxazoline)-*block*-poly(dimethylsiloxane)-*block*-poly(2-methyl-2-oxazoline) (PMOXA-*b*-PDMS-*b*-PMOXA, Figure 1A, **1**) was synthesized as previously published

(Figure S1, Table S1),[34,35] and the PDMS-heparin block copolymer (Figure 1A, **2**) was synthesized by coupling a commercial PDMS block with commercial heparin polysaccharide (Figures S2, S3). A critical step was the solubilization of heparin in organic solvents, which is not possible with the commercial sodium salt of heparin, but was needed for PDMS-heparin synthesis and nanomimic formation. Therefore, it was first hydrophobized by ion exchange from sodium to tetrabutylammonium,[36] which exchanged again with sodium during nanomimic purification. ^{1}H NMR after reaction, purification, and ion exchange indicated successful coupling of PDMS with heparin (Figure S3). The reductive amination used for PDMS-heparin synthesis is a mild reaction; the reducing agent is specific to imines.[37] This specific reaction ensured that heparin was modified with PDMS only at its natural anchor point, leaving the rest of the chain unmodified. Farndale microassays, in which positively charged dye molecules align on heparin chains resulting in a metachromatic shift in the absorption spectrum, were performed in ethanol to obtain a rough estimation of the number of saccharide units per PDMS chain (5 kDa). Tetrabutylammonium heparin in ethanol was used to generate a calibration curve (Figure S4), and by comparing to the absorption values found for PDMS-heparin the number of saccharide units per PDMS chain was calculated to be about 25 (in total 11 kDa).

Preparation and Characterization of Nanomimics. Nanomimics were self-assembled by the bulk rehydration technique using a mixture of PMOXA-*b*-PDMS-*b*-PMOXA with 25% (w/w) PDMS-heparin block copolymer. Since heparin (mean 11 kDa, 25 saccharide units) of PDMS-heparin is a longer polymer than PMOXA (max. 0.8 kDa, 5 to 9 oxazoline units) of PMOXA-*b*-PDMS-*b*-PMOXA and PDMS blocks were similar in both copolymers (mean 5 kDa, 63 siloxane units), only a small part of heparin was shielded by PMOXA, while the rest was accessible for protein interaction (Figure 1D,E).

Dynamic light scattering (DLS) revealed hydrodynamic nanomimic diameters (D_H) of about 132 ± 34 nm (average of eight independent samples ± standard deviation) (Table S2). DLS and static light scattering (SLS) performed on four representative nanomimic samples provided R_g/R_H values of ρ = 0.90−0.99, as expected close to the value of 1.0 for ideal hollow spheres (vesicles)[38] and thus indicating the vesicular structure of nanomimics (Table S2). Transmission electron microscopy (TEM) and cryogenic-TEM (cryo-TEM) confirmed these vesicle sizes and illustrated the membranous structure of these nanomimics (Figure 1B,C, Figure S5). TEM micrographs showed collapsed nanomimics (D = 111 ± 38 nm, Figure 1B), which clearly distinguished them from filled nanoparticles. Nanomimics retained their spherical structure (D = 101 ± 33 nm, Figure 1C) during cryo-TEM imaging and revealed a vesicle-in-vesicle structure and a membrane thickness of 10.9 ± 1.4 nm. By increasing the PDMS-heparin content in nanomimics, a transition to micelles was observed. Nanomimics prepared with increasing PDMS-heparin content (35−65% w/w) yielded mixtures of polymersomes and worm-like micelles (35%, 45%) and finally aggregated micelles (55%, 65%) (Figure S6). Self-assembly of PDMS-heparin copolymer alone yielded aggregated micelles with a D_H of about 83 ± 26 nm (DLS) (Table S2, Figure S5D,H). This demonstrates that nanomimics (25% w/w) consist of a real mixture of both copolymers; otherwise we would have observed aggregated micelles in the samples containing those nanomimics. Nanomimics with 25% (w/w) PDMS-heparin were used in all subsequent experiments. Furthermore, stopped-flow measurements on nanomimics revealed their permeability for water but not solutes. This was concluded due to nanomimic shrinkage upon applied osmotic pressure by doubling the salt concentration outside of nanomimics (Figure S7).[35]

Hydrophilic sulforhodamine B (SRB) was encapsulated in the aqueous core of nanomimics for visualization, and both D_H and the concentration of the nanomimics were obtained with fluorescence correlation spectroscopy (FCS) by comparing diffusion time of the free dye with that of the encapsulated dye (Figure S8). The concentration of the nanomimics obtained by FCS was 71 ± 18 nM (2.8 mg/mL PMOXA-*b*-PDMS-*b*-PMOXA, 0.93 mg/mL PDMS-heparin); this value was subsequently used to calculate the number of nanomimics necessary to obtain an effect in the antimalarial assay (Figure 4).

Farndale microassays in aqueous solution were performed to quantify the amount of surface-accessible heparin on nanomimics after purification (Figure S9). Calibration curves (Figure S9A) were produced with the same heparin solution that was subsequently used in *in vitro* assays (Figure 4) to ensure comparability of assays. PMOXA-*b*-PDMS-*b*-PMOXA polymersomes did not influence the absorbance spectrum of the dye in the range of interest (Figure S9B). Due to the random character of the self-assembly process underlying nanomimic formation, not all PDMS-heparin added led to surface-exposed heparin in the final nanomimics; a fraction of the heparin chains will face toward the vesicle core, a few will be hidden in the membrane or in the nanomimic core (vesicle-in-vesicle structures), and a few free PDMS-heparin or free heparin chains not incorporated in the membrane were removed during purification. However, Farndale microassays allowed us to quantify the amount of heparin exposed at the outer surface of the nanomimics. Importantly, nanomimic formation yielded detectable amounts of heparin being incorporated in the membrane after purification, whereas formation with PMOXA-*b*-PDMS-*b*-PMOXA and the tetrabutylammonium salt of heparin did not (Figure S9B). In total, three independent PDMS-heparin and three PMOXA-*b*-PDMS-*b*-PMOXA batches

were used (Table S1). Nanomimics1 and micelles1 were built from the same batch of PDMS-heparin; nanomimics2 and micelles2 were made from two other batches of PDMS-heparin. Typical nanomimic samples, theoretically containing 2.5 mg/mL PMOXA-*b*-PDMS-*b*-PMOXA and 0.83 mg/mL PDMS-heparin copolymer, yielded 57 ± 13 μg/mL (mean ± standard deviation) surface-exposed heparin after purification (Table S2). If combined with the nanomimic concentrations obtained by FCS measurements, there are about 74 ± 30 heparin chains (11 kDa) exposed on the outer surface of one nanomimic. Zeta potential measurements performed on nanomimics (−32.4 ± 4.1 mV, average of eight nanomimic samples) and control polymersomes (+5.4 ± 0.2 mV) confirmed the presence of negatively charged groups on nanomimics in contrast to pure PMOXA-*b*-PDMS-*b*-PMOXA vesicles.

To validate the toxicity of nanomimics on cultured cells, a cell viability test was performed using HeLa cells and a representative nanomimic sample (2.9 mg/mL PMOXA-*b*-PDMS-*b*-PMOXA, 49.3 μg/mL accessible heparin) (Figure S10). This test demonstrated the absence of any cell toxicity of nanomimics up to the maximum concentration of 290 μg/mL PMOXA-*b*-PDMS-*b*-PMOXA and 4.9 μg/mL surface-exposed heparin, which was an even higher concentration than the highest concentration used in the antimalarial assays (Figure 4).

Nanomimics Bind *Plasmodium* Merozoite Proteins Involved in Initial Attachment. FCS also allows the analysis of protein binding to nanoobjects by comparing diffusion times of freely diffusing and bound proteins labeled with fluorescent molecules.[39] For the FCS measurements, Oregon Green was used to label the *P. falciparum* (clone 3D7) major surface protein 1-42 (*Pf*MSP1$_{42}$-OG488), which has been identified as the ligand for heparin-like receptors.[9] The difference in diffusion times between *Pf*MSP1$_{42}$-OG488 and *Pf*MSP1$_{42}$-OG488 bound to nanomimics was used to verify that the surface of nanomimics contained accessible heparin molecules and that they were able to bind merozoite proteins (Figure 1D,E). No binding of *Pf*MSP1$_{42}$-OG488 occurred with polymersomes without heparin. In contrast, nanomimics and PDMS-heparin micelles bound significant amounts of *Pf*MSP1$_{42}$-OG488 (from 5 up to 12 *Pf*MSP1$_{42}$-OG488 per nanomimic, Figure 1D,E). Therefore, strong multivalent binding of several *Pf*MSP142 on one parasite with several heparin chains on one nanomimic is possible, which is an important parameter for invasion inhibition. Furthermore, the interaction of *Pf*MSP1$_{42}$-OG488 with heparin on artificial membranes seems to be a high-affinity interaction; otherwise no binding would have been observed by FCS.[40] Although heparin has a slightly different structure compared to heparan sulfate, the FCS results provided evidence for high-affinity binding in contrast to previous suggestions that the initial attachment of merozoites to RBCs is a low-affinity interaction.[32] Thus, it is possible that the low abundance of heparan sulfate on RBCs (~2000 chains per RBC)[33] providing only one or a few sugar chains per merozoite for initial attachment is sufficiently strong not only to attach to the RBC but also to allow for subsequent interaction with other receptors for stronger attachment and subsequent reorientation (Scheme 1).

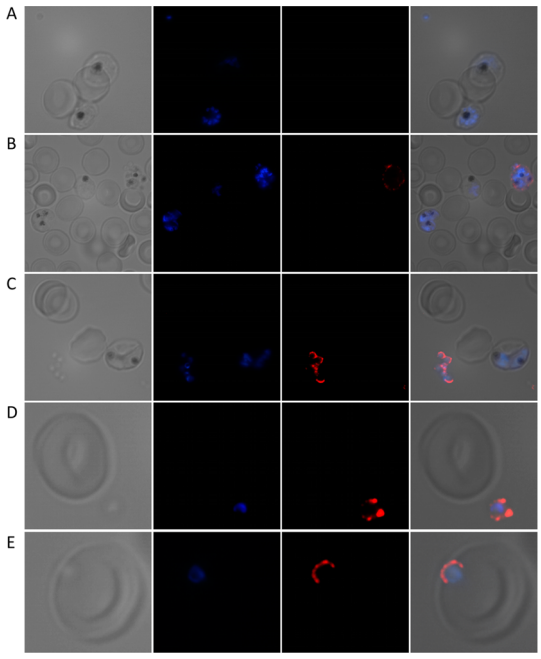

Figure 2. Inhibition of merozoite invasion by nanomimics. (A) Control polymersomes (PMOXA-*b*-PDMS-*b*-PMOXA only) did not bind to merozoites, RBCs, and iRBCs. (B) SRB-filled nanomimics (red) bound to schizonts during merozoite egress, but not to intact iRBCs (all stages) and RBCs; iRBCs and RBC appear normal. (C−E) Merozoites (blue) were inhibited by nanomimics (red) from entering into fresh RBCs. Left: DIC, middle: DAPI (blue) and SRB (red), right: merge.

Nanomimics Block Invasion of and Expose *Plasmodium* Merozoites. To test whether our nanomimics could competitively bind freshly egressed merozoites and therefore block RBC invasion *in vitro*, we incubated a mixture of RBCs and late stages of infected RBCs (iRBCs) with these nanomimics for 3 h. During this time, merozoites start to be released and invade new RBCs. After incubation with fluorescent nanomimics fluorescence imaging showed both binding of nanomimics to merozoites and lack of RBC invasion (Figure 2C to E). Extracellular merozoites lose their invasive capacity after 5 min at 37 °C;[41] therefore if merozoites with surface-bound nanomimics appear in culture, they already lost their ability to infect new RBCs (Figure 2C to E). In addition, agglutination of merozoites and nanomimics (Figure 2C) and nanomimic binding to iRBC just during merozoite egress were observed (Figure 2B), whereas intact iRBCs and RBCs did not bind nanomimics. Polymersomes without heparin did not bind any of the cells present (RBCs, iRBCs, or

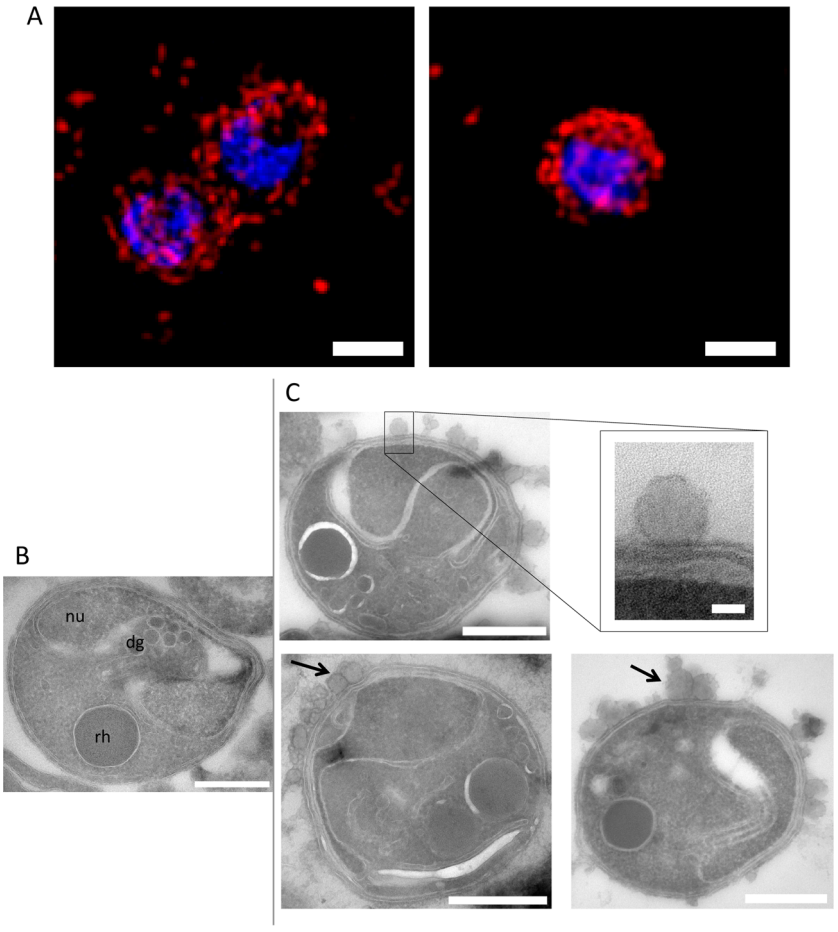

Figure 3. Merozoites bound with nanomimics. (A) Projections of merozoites (DAPI, blue) blocked by SRB-filled nanomimics (red, scale bars, 1 μm) recorded with super-resolution 3D structured illumination microscopy (3D-SIM). (B) TEM of an ultrathin section of a control merozoite (scale bar, 500 nm). (C) TEM of ultrathin sections of merozoites with nanomimics on the surface (scale bars, 500 nm) and higher magnification of a surface-bound nanomimic (scale bar 50 nm). Lipid membranes (light) can be distinguished from the polymer membrane of nanomimics (dark), and the size of the surface-bound nanomimics is in agreement with the diameters of nanomimics (Figure 1B,C). Rhoptries (rh), nucleus (nu), and dense granules (dg) of merozoites can be seen clearly. Some nanomimics are indicated with a black arrow.

merozoites) and could therefore not block invasion; only very few merozoites can be found in the controls (Figure 2A).

The merozoite–nanomimic interaction was further examined by super-resolution 3D structured illumination microscopy (3D-SIM) and electron microscopy (EM) of ultrathin sections of merozoite–nanomimic complexes (Figure 3). 3D reconstruction of merozoites with surface-bound nanomimics showed that several dozens of nanomimics bound to a single merozoite (Figure 3A). The EM images of ultrathin sections revealed nanomimics attached to the outer membrane of merozoites (Figure 3C), which was not found in a preparation without nanomimics (Figure 3B). This revealed that nanomimics blocked the docking sites on merozoites, whereas no fusion of nanomimic and parasite membrane occurred.

Efficacy of Invasion Inhibition by Nanomimics. The inhibitory effect of nanomimics on the parasite life cycle was determined by a growth inhibition assay using a *P. falciparum* (clone 3D7) suspension culture in 24-well plates, which better mimics the *in vivo* situation by using suspension cultures with a higher hematocrit than usually used for measurements of drug effects (typically 1%).[42] Invasion–inhibition curves with free heparin, nanomimics, and PDMS-heparin micelles (Figure 4) show a significant difference in IC_{50} values between free heparin and nanomimics or PDMS-heparin micelles (Figure 4A). All parasites were blocked at the highest heparin, nanomimic, or micelle concentrations.

IC_{50} values dramatically decreased from 37.4 $\pm$ 4.7 μg/mL (2.5 μM for free heparin) to 0.197 $\pm$ 0.047 μg/mL for the best preparation of nanomimics (13 nM of heparin on nanomimics2) (Figure 4B). This corresponded to a decrease in IC_{50} value of more than 2 orders of magnitude (Figure 4C), which indicates a very highly efficient inhibitory effect of the nanomimics. The highest concentration of nanomimics tested contained about 60 μg/mL of the polymersome-forming PMOXA-*b*-PDMS-*b*-PMOXA and about 1 μg/mL surface-accessible heparin. Polymersomes consisting of

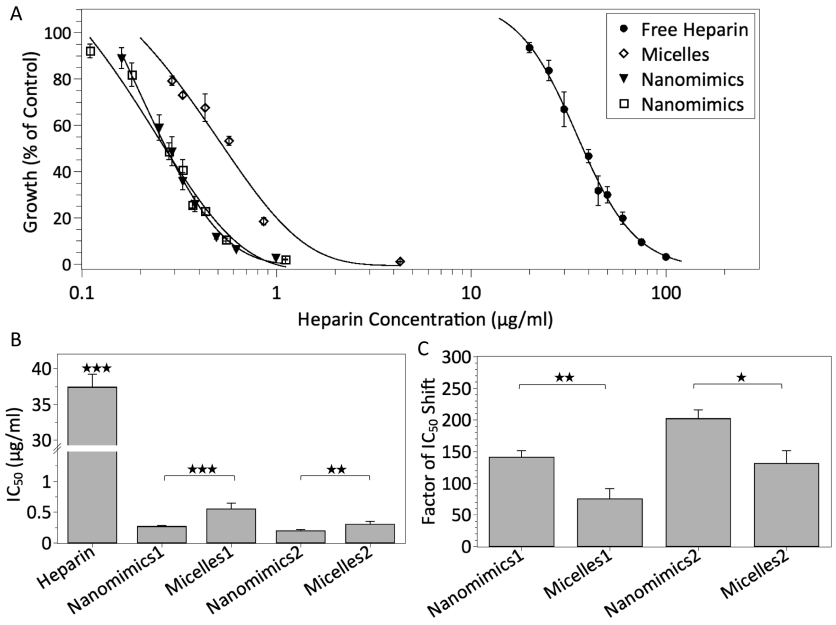

Figure 4. Growth inhibition by free heparin and nanomimics. (A) Free heparin inhibits growth of *P. falciparum* (3D7) in the suspension assay. Micelles built from PDMS-heparin and nanomimics inhibit merozoite invasion more efficiently than free heparin (data from five independent invasion inhibition experiments; all data points are mean growth ± standard error from at least three duplicate assays for each), presented as percentage of control (PBS)). (B) IC_{50} values for free heparin (n = 7) compared to heparin-loaded nanomimics ($n1$ = 9, $n2$ = 12) or micelles ($n1$ = 4, $n2$ = 3), indicating the importance of nanostructured heparin for increased activity. Nanomimics1 and micelles1 were built from the same batch of PDMS-heparin; nanomimics2 were made from two other batches of PDMS-heparin (mean values ± standard error for three independent experiments for each sample). (C) Comparison of nanomimics and micelles expressed as factor of x difference in IC_{50} values for nanostructures compared to free heparin (mean values ± standard error for three independent experiments for each sample). Statistics were analyzed using Student's t-test: $^{\star}p < 0.05$, $^{\star\star}p < 0.01$, $^{\star\star\star}p < 0.001$.

PMOXA-*b*-PDMS-*b*-PMOXA without PDMS-heparin or PMOXA-*b*-PDMS-*b*-PMOXA vesicles with encapsulated tetrabutylammonium heparin had no effect on the parasite life cycle at similar concentrations (60 μg/mL); parasitemia reached the same values as in control wells with PBS only. A solution of free tetrabutylammonium heparin after size exclusion chromatography (as we do with nanomimics) was also not active at concentrations similar to the highest heparin concentration used in the case of nanomimics (about 1 μg/mL). The IC_{50} value for free heparin was 2-fold higher than previously published,[9] most probably due to the higher hematocrit (5%) and suspension culture. Nanomimics with different ratios of PDMS-heparin to PMOXA-*b*-PDMS-*b*-PMOXA were also tested in order to find the optimum mixture. Nanomimics containing 25% (w/w) PDMS-heparin provided the best balance in terms of efficacy and control over self-assembly (exclusively spherical vesicles; Figure 1B,C, Figures S5, S6). Nanomimics were also significantly more effective than micelles self-assembled from PDMS-heparin only, most likely because the membranous structure of the nanomimics allowed lateral diffusion of receptors for multivalent interactions.[5] This demonstrates the advantage of using membranous nanomimics compared to micellar or solid nanostructures.

Considering that the active inhibitors are nanomimics themselves—no drug is released from the nanostructure—the IC_{50} value can also be presented in "nanomimic concentrations". The nanomimic concentration was determined by FCS in PBS (71 ± 18 nM for nanomimics at 2.8 mg/mL PMOXA-*b*-PDMS-*b*-PMOXA and 0.93 mg/mL PDMS-heparin concentrations). Combining this value with the antimalarial assay results in an IC_{50} value of 0.27 ± 0.09 nM for the nanomimics (five independent samples, three invasion inhibition assays). Therefore, one nanomimic is about as active as 10 000 heparin chains. This significantly higher inhibitory activity of nanomimics compared to free heparin (>2 orders of magnitude) is explained by multivalent interactions between a multitude of heparin molecules exposed on a single nanomimic with a multitude of *Pf*MSP1$_{42}$ molecules on each merozoite (max. 12 *Pf*MSP1$_{42}$-OG488 per nanomimic measured), confirming results from binding assays. Indeed, nanomimics represent "macroscopic" objects when compared to free heparin, and thus the binding of a few nanomimics was sufficient to block merozoites from entering fresh RBCs, while a very large number of free heparin molecules (~10 000 times more) was required for such an effect. Our nanomimics block pathogens using the combined effect of a spatial architecture with a specific, exposed receptor of host cell membranes.

CONCLUSIONS

Nanomimics of host cell membranes were successfully produced by a simple self-assembly procedure

without postformation modifications, which uses a mixture of polymersome-forming block copolymer with a copolymer that consists of a hydrophobic block and a specific host cell receptor. The resulting 3D-nanoobjects (nanomimics) very efficiently blocked invasion of RBCs by *P. falciparum* merozoites as compared to soluble receptors, which can be explained by strong multivalent binding of nanomimics to merozoites. This might offer an interesting treatment option for severe malaria when prevention of reinvasion of parasites is of highest priority. Simultaneously, similar to soluble heparin, such nanomimics treatment would be expected to reverse the two major pathogenic events in *P. falciparum* infections—sequestration and rosetting—*in vitro* and *in vivo* and thus immediately would reduce pathology.[10,11]

As an additional benefit, our nanomimic strategy will keep a large number of merozoites artificially extracellular after egress. Circulation of a large number of free merozoites does not naturally occur, and it might be speculated whether these merozoites bound to nanomimics represent a strong immunogen and might elicit a strong immune response against all merozoite antigens. Because this would happen during a natural or controlled[43] infection, it would avoid many problems associated with subunit or attenuated merozoite vaccines.[18] However, it remains to be tested as to whether such induced immunity is superior to responses derived from any natural infection or from recombinant antigens.

Thus, our strategy of interrupting the parasite life cycle using nanomimics and then subsequently eliciting an immune response represents a promising alternative to current drug treatment and vaccination strategies.[43] Further, nanomimics offer theoretically a unique possibility of encapsulating high concentrations of adjuvants or other immune modulators, which could be released after phagocytosis to enhance immunogenicity. We have used these nanomimics to interrupt the life cycle of malaria parasites as a proof of principle, but a variety of other pathogens also use host cell heparan sulfate for initial attachment;[6] therefore this technology might be much more widely applied to inhibit other infections.

MATERIALS AND METHODS

PMOXA-*b*-PDMS-*b*-PMOXA (1) Synthesis. PMOXA-*b*-PDMS-*b*-PMOXA (**1**) was synthesized according to previously published protocols.[34,35,44] Briefly, bifunctional poly(dimethylsiloxane) (PDMS from ABCR GmbH, Karlsruhe, Germany) was vacuum stripped in a Schlenkflask overnight. Anhydrous hexane was subsequently added, and the stirred solution was dried by bubbling argon through it for 1 h. After bubbling, freshly distilled triethylamine (TEA) was added, and the mixture was cooled to −20 °C. PDMS was then reacted with trifluoromethanesulfonic acid (Tfsa) for 3 h at −20 °C, resulting in a bifunctional triflic PDMS macroinitiator. The reaction mixture was filtered through a cooled G4 filter under argon. From the filtrate hexane was removed under vacuum and replaced by dry ethyl acetate. Adding distilled 2-methyl-2-oxazoline resulted in a cationic ring-opening polymerization of poly(2-methyl-2-oxazoline) (PMOXA) on the PDMS macroinitiator. Termination was performed after 60 h at 40 °C by adding a 2:8 mixture of TEA/water, resulting in bifunctional OH-terminated PMOXA-*b*-PDMS-*b*-PMOXA. Finally, the solvent was removed by vacuum distillation. Purification was performed by resolubilizing the polymer in a 1:1 ethanol/water mixture and ultrafiltration through a 5 kDa membrane. The final product was dried under vacuum.

PDMS-Heparin (2) Synthesis. Heparin sodium salt from porcine intestinal mucosa (15 kDa, 197 U/mg, 375095) was purchased from Merck KGaA (Darmstadt, Germany), and aminopropyl-terminated poly(dimethylsiloxane) ($PDMS(NH_2)_2$, **S1**) (5 kDa, AB109371) from ABCR GmbH (Karlsruhe, Germany).

The tetrabutylammonium salt of heparin (**S2**, Figure S2) was obtained using a published protocol.[36] Briefly, 500 mg of heparin sodium salt was dissolved in a minimum amount of water (approximately 3 mL) and passed through a freshly packed Dowex Marathon MSC column (H^+ form, 6 mL, Sigma-Aldrich, 428787). The pH was adjusted to pH 7 using a tetrabutylammonium hydroxide solution (54.0−56.0% in H_2O, Sigma-Aldrich, 86863). After reducing the volume on a rotary vacuum evaporator, the product was dialyzed against water for at least 48 h (Spectrum Laboratories Inc., Rancho Dominguez, CA, USA, MWCO 3.5−5 kDa). The product was subsequently dried under vacuum. To use as a control in the antimalarial assay, tetrabutylammonium heparin was first precipitated in cold diethyl ether, dried under vacuum, dissolved in PBS, and then passed through a size exclusion column (Sepharose 2B, Sigma-Aldrich, 2B300) equilibrated in PBS. The final concentration of heparin was then determined using the Farndale microassay.

For PDMS-heparin (**2**, Figure S2) synthesis, 100 mg of **S2** (∼22 kDa) was dissolved in a 50 mL round-bottom flask in 25 mL of dichloromethane (DCM), and a hundred-fold excess of **S1** was added under stirring. Furthermore, a 10-fold excess of 2-picoline borane (Sigma-Aldrich, 654213) was dissolved in a small amount of DCM, added to the reaction mixture, and stirred for 7 days at room temperature (25 °C). After the third and fifth day of the reaction another 10-fold excess of 2-picoline borane was added, respectively. After 7 days, DCM was evaporated on a rotary evaporator and the product was washed in diethyl ether. The washed product was dried under vacuum and redissolved in a minimum amount of ethanol. Adding the solution dropwise into 4 × 15 mL of diethyl ether in glass centrifugal tubes precipitated the product; unreacted **S1** and reducing agent were soluble in diethyl ether. The precipitate was collected by centrifugation for 5 min (2000 RCF) and discarding the supernatant. This precipitation process was repeated two times. The final product was dissolved in ethanol, filtered, and dried under vacuum. For ^1H NMR about 20 mg of the product was dissolved in 10% ethanol and passed through a freshly packed Dowex Marathon MSC column (Na^+ form, 2 mL, Sigma-Aldrich, 428787), and the volume was reduced to about 2 mL on a rotary evaporator, dialyzed against water for 24 h (Spectrum Laboratories Inc., Rancho Dominguez, CA, USA, MWCO 8−10 kDa), dried under vacuum, and redissolved in D_2O/acetone-d_6 (v/v 3:1).

Polymersome and Nanomimic Formation. Control polymersomes (PMOXA-*b*-PDMS-*b*-PMOXA only) were formed by the film rehydration technique.[44] A 1 mL amount of PMOXA-*b*-PDMS-*b*-PMOXA (6 mg/mL in ethanol) was put in a 5 mL round-bottom flask, and ethanol was removed on a rotary evaporator (100 mbar, 40 °C, 120 rpm). Subsequently, the thin polymer film was rehydrated using PBS or 1 mM SRB (Sigma-Aldrich, S1402) in PBS and stirred at least overnight.

Nanomimics were prepared using the bulk rehydration technique.[44] PMOXA-*b*-PDMS-*b*-PMOXA (6 mg/mL) and PDMS-heparin (4 mg/mL) were dissolved in ethanol (both yielded clear solutions) and mixed in a 5 mL round-bottom flask in the desired ratio. The solvent was evaporated on a rotary

evaporator (100 mbar, 40 °C, 120 rpm), and the film was further dried at high vacuum overnight. The polymer film was subsequently destroyed using a spatula. The bulk polymer was hydrated in PBS and stirred for at least 12 h. To yield fluorescent nanomimics, the polymer mixture was hydrated using a 1 mM SRB (Sigma-Aldrich, S1402) solution in PBS. To use as a control in the antimalarial assay, tetrabutylammonium heparin, which was first precipitated in diethyl ether, dried under vacuum, and dissolved in ethanol, was encapsulated in control polymersomes by adding 0.54 mL (4 mg/mL in ethanol) of the tetrabutylammonium heparin solution to 1 mL of PMOXA-*b*-PDMS-*b*-PMOXA (6 mg/mL in ethanol) with subsequent vesicle formation as described above for nanomimics (bulk rehydration[44]).

Micelle Formation. PDMS-heparin micelles were formed similar to nanomimics but by using only PDMS-heparin (100%) instead of a mixture with PMOXA-*b*-PDMS-*b*-PMOXA.

Nanostructure Extrusion and Purification. The polymersome, nanomimic, and micelle solutions were extruded 15 times through a 0.1 μm Nuclepore track-etch membrane (Whatman, GE Healthcare, UK) using a LIPEX extruder (Northern Lipids Inc., Canada). The final solution of nanostructures was passed through a size-exclusion column containing Sepharose 2B (Sigma-Aldrich, 2B300) equilibrated with PBS.

Protein Labeling. Water-soluble proteins were fluorescently labeled *via* amine groups using Oregon Green 488 carboxylic acid, succinimidyl ester, 5-isomer (OG488-NHS, Invitrogen, Carlsbad, CA, USA, O-6147) using established protocols (Invitrogen). The buffer of *P. falciparum* major surface protein 1-42 (*Pf*MSP1$_{42}$ (3D7)) was exchanged with 0.1 M carbonate buffer (pH 8.3) at a concentration of 2 mg/mL by using Amicon Ultra-0.5 mL (10K) centrifugal filters. OG488-NHS was dissolved in water-free DMSO (19.6 mM), and a 12-fold excess of OG488-NHS was added to the protein solution. After shaking for at least 2 h at room temperature, free OG488 was separated from labeled proteins on HiTrap desalting columns (Sephadex G25) using PBS as running buffer. The labeled proteins were stored in aliquots at −20 °C.

Farndale Microassay. Farndale microassays were performed based on Farndale *et al.*[45] with slight modifications. To obtain the amount of saccharide units per PDMS chain (5 kDa), an ethanolic solution of dimethylmethylene blue (DMMB) was prepared (15.8 μg/mL). A 250 μL sample of this solution was pipetted into each well of a 96-well plate, and 50 μL of ethanol (blank), tetrabutylammonium heparin in ethanol (100, 50, 25, 10 μg/mL), and PDMS-heparin in ethanol (100 μg/mL, 50 μg/mL) were mixed into each well in duplicates. The UV−vis absorbance was measured from 495 nm to 605 nm immediately after mixing. The tetrabutylammonium heparin standard curve was generated using the absorbance at the peak maximum at 565 nm. Absorbance at 565 nm of the PDMS-heparin samples and the calibration curve were used to calculate the relative tetrabutylammonium heparin content (*R*) in PDMS-heparin and the molecular weight of tetrabutylammonium heparin (MW) per PDMS while assuming a constant length of PDMS (5 kDa) and using

$$R = \frac{c(\text{assay})}{c(\text{added})} = \frac{\text{MW}}{(\text{MW} + 5\ \text{kDa})}$$

The number of tetrabutylammonium saccharide units per PDMS chain was obtained using MW and a tetrabutylammonium saccharide unit molecular weight of 440 g/mol (300 g/mol[36] × 3/2).

For Farndale microassays in aqueous solutions, the DMMB solution was prepared as suggested.[46] A 250 μL sample of the DMMB solution was pipetted into 96-well plates. A 50 μL amount of PBS, heparin standards (20, 10, 7.5, 5, 2.5 μg/mL), and diluted nanomimic and control polymersome samples (typically 5-fold diluted) were mixed with the DMMB solution in duplicates. The UV−vis absorbance was measured from 395 nm to 595 nm immediately after mixing. The heparin standard curve was generated using the absorbance at 525 nm, and this curve was used as a calibration curve. In the nanomimic samples a baseline correction (exponential decay) was performed and the corrected absorbance value at 525 nm was used to calculate the amount of surface-accessible heparin.

UV−Vis Spectrometry. UV−vis absorbance measurements were performed on a SpectraMax Plus M5e (Molecular Devices, Sunnyvale, CA, USA) using 0.1 mL cuvettes or 96-flat-bottom-well plates.

Nuclear Magnetic Resonance. ^{1}H NMR spectra were recorded on a Bruker DPX-400 NMR spectrometer in D_2O, D_2O/acetone-d_6 mixture, or $CDCl_3$ at room temperature. The spectrometer was operated at 400 MHz, and 16 or 128 NMR cycles were recorded for each sample.

Gel Permeation Chromatography. Gel permeation chromatography (GPC) was performed on a Viscotek GPCmax system equipped with two PLgel Mixed-c 5 μm columns (300 × 7.5 mm) and THF as eluent (flow rate = 1 mL min^{-1}) at 40 °C and recorded by refractive index. Polymer molecular weights and polydispersity indices were determined using polystyrene standards for calibration.

Transmission Electron Microscopy. Nanostructure samples were negatively stained with 2% uranyl acetate for TEM imaging. Ultrathin sections of parasites were stained with a mixture of 4% uranyl acetate/methylcellulose (ratio 1:9). Imaging was carried out on a transmission electron microscope (Philips CM100) at an acceleration voltage of 80 kV. Size measurements were performed using ImageJ software.

Cryogenic Transmission Electron Microcopy. A 4 μL amount of nanomimic sample (3 mg/mL) was adsorbed on a holey carbon-coated grid (Quantifoil, Germany), blotted with a Whatman 1 filter paper and vitrified in liquid nitrogen-cooled liquid ethane using an FEI Vitrobot MK4 (FEI Company, The Netherlands). Frozen grids were transferred to a Philips CM200-FEG electron microscope, which was operated at an acceleration voltage of 200 kV. Digital electron micrographs were recorded with a 4k × 4k TemCam-F416 CMOS camera (TVIPS Company, Germany).

Zeta Potential. Zeta potential measurements were performed using a Zetasizer Nano ZSP (Malvern Instruments Ltd., UK) at 20 °C. Nanomimics or control polymersomes (about 3 mg/mL polymer concentration) prepared and purified in PBS were 40-fold diluted in 300 mM glucose (75 μg/mL polymer and less than 5 mM salt).

Fluorescence Correlation Spectroscopy. FCS measurements were performed on a commercial Confocor2 (Carl Zeiss, Jena, Germany) using an Ar+ laser for the 488 nm wavelength and a HeNe laser for 543 nm. The laser beam was focused onto the sample through a 40× C-Apochromat water immersion objective with a numeric aperture of 1.2 and the appropriate filter sets. Finally, the fluorescence intensity was recorded with an avalanche photodiode (APD). All measurements were performed at 20 °C.

Typically, 5 μL samples were used. Measurement series of 30 × 5 s (fast diffusing species) or 30 × 10 s (slow diffusing species) were taken for each sample. Raw data were processed with the ConfoCor3 software. R Statistics was used for normalization and graphs. The following fit function was used to fit samples with one component and including a triplet state:

$$G(\tau)_{\text{fit}} = 1 + \left(1 + \frac{T}{1-T}\, e^{-\tau/\tau_{\text{trip}}}\right)\frac{1}{N}\left[\frac{1}{1+\frac{\tau}{\tau_D}}\,\frac{1}{\sqrt{1+R^2\frac{\tau}{\tau_D}}}\right]$$

τ_D is the diffusion time. *T* represents the fraction of fluorophores in triplet state with the corresponding triplet time τ_{trip}. *N* is the number of particles and *R* the structural parameter. *R* was set to 5 if fit results yielded *R* smaller than 3 or bigger than 8. The relation between the *x*−*y* dimension of the confocal volume (ω_{xy}) and τ_D was used to calculate diffusion coefficients (*D*).

$$\tau_D = \frac{{\omega_{xy}}^2}{4D}$$

The Einstein−Stokes equation was utilized to calculate hydrodynamic radii (R_H). k_B is Boltzmann's constant, *T* the absolute temperature, and η the viscosity of the

surrounding medium.

$$D = \frac{k_B T}{6\pi\eta R_H}$$

R_H was calculated for each of the 30 curves, and data are presented as mean ± standard deviation. To obtain nanomimic concentrations, calibration of the confocal volume was needed. This was obtained by measuring a series of dye solutions with known concentrations from 1 to 100 nM. A linear fit of dye concentration *versus* N—obtained from amplitudes of FCS curves—yielded the size of the confocal volume (approximately 0.5 fL). This calibrated value was subsequently used to determine nanomimic concentrations.

For binding studies, *Pf*MSP1$_{42}$-OG488 was mixed with controls or nanomimics, incubated under shaking at 37 °C for 2 h, cooled to RT (20 °C), put on the cover slide, and incubated 5 min, and FCS curves were recorded. Autocorrelation curves that could not be fitted due to big diffusing aggregates were excluded from the mean (max. 3 of 30 curves, 10%). Brightness (counts per molecule, CPM) of free *Pf*MSP1$_{42}$-OG488 was compared to CPM obtained from the mixtures with nanostructures in order to calculate the number of *Pf*MSP1$_{42}$-OG488 per nanostructure.

Static and Dynamic Light Scattering. Dynamic light scattering was performed on a Zetasizer Nano ZSP (Malvern Instruments Ltd., UK) at 20 °C. SLS/DLS was carried out to determine the hydrodynamic radius (R_H), the radius of gyration (R_g), and the value $\rho = R_g/R_H$ of nanomimics in solution. SLS and DLS experiments were performed on an ALV goniometer (ALV GmbH, Germany), equipped with an ALV He−Ne laser (λ = 632.8 nm). Measurements were performed in 10 mm cylindrical quartz cells at angles of 30−140° at 20 °C. Data processing was performed using ALV static and dynamic fit and plot software (version 4.31 10/01). SLS data were processed using the Berry model.

Stopped-Flow Measurements. The effect of osmotic pressure on nanomimic size was determined using a stopped-flow apparatus (Bio-Logic SAS, France). Changes in light scattering were monitored at an emission wavelength of 600 nm. As a control, nanomimics in 1× PBS were mixed equally with 1× PBS. Osmotic pressure was generated using 2× PBS as the mixing medium with nanomimics in 1× PBS. At least four measurements were conducted for each mixture at 20 °C. Experimental curves were fitted using exponential fits in QtiPlot (http://soft.proindependent.com/qtiplot.html).

Viability MTS Assay. HeLa cells (2000 cells per well) were seeded in a 96-well plate and incubated at 37 °C, 5% CO_2 for 24 h in DMEM containing 10% fetal calf serum and 1% penicillin/streptomycin. After 24 h, nanomimics were added to triplicate wells at concentrations ranging 50−300 μg/mL in a total volume of 100 μL per well (90 μL of media mixed with 10 μL of nanomimic solution in PBS). Cells were incubated in the presence of nanomimics for an additional 24 h. Cell viability was determined using the MTS assay. Briefly, 20 μL of MTS assay solution was added to each well and incubated at 37 °C for 3 h. Cell viability was determined by measuring absorbance at 490 nm using a microplate reader SpectraMax Plus M5e (Molecular Devices) and comparing to a PBS control (100% cell viability) to obtain the percentage of living cells. All samples were corrected against controls containing only media and PBS or an SRB solution in PBS.

Suspension Culture Assay. *Plasmodium falciparum* 3D7 strain was maintained in culture as described elsewhere.[47] Malaria culture medium (MCM) was RPMI medium supplemented with 0.5% Albumax.[48] Synchronization was performed using 5% sorbitol.[49]

Invasion inhibition experiments were carried out in standard 24-well flat-bottom culture plates (Falcon 353047, Becton Dickinson, NJ, USA). Starting parasitemia was about 0.1% ring/trophozoite stages at 5% hematocrit in MCM, and parasitemia reached ∼2−4% after 96 h. Total volume added to each well was 500 μL of parasite culture plus 55 μL of PBS or test samples. Plates were placed in a plastic box with wet paper (for humidification) and cultured under continuous and simultaneous rocking (140 rpm, ProBlot 25 Rocker, Labnet International Inc., NJ, USA) and shaking (105 rpm, Lab-Therm LT-W, Kühner, Switzerland) at 37 °C for 96 h by fixing the ProBlot 25 Rocker onto the shaking plate of the Lab-Therm shaking incubator. The maximum tilt angle was increased to 15° by putting one side of the plastic box on a 3 cm thick spacer. This setup ensures continuous suspension of RBCs and iRBCs over the 96 h incubation period. Each sample was tested in at least three independent assays in duplicates. After 96 h, parasitemia was determined by flow cytometry (FACSCalibur, BD Biosciences) using dihydroethidium to stain parasite DNA. In total, 100 000 cells were counted for each well. Data are presented as mean growth ± standard error with respect to PBS controls. Statistical comparison of free heparin *versus* nanostructured heparin was performed using Student's *t*-test (two-tailed, type 2) in Microsoft Excel. Graphs were drawn using QtiPlot (http://soft.proindependent.com/qtiplot.html). To obtain IC_{50} values, experimental growth inhibition curves were fitted using logistic or exponential curves in QtiPlot.

Preparation of Parasites for Fluorescence Microscopy. Mature 3D7 parasites (trophozoites/schizonts) were purified by Percoll density gradient.[50] Then, purified late stages were mixed again with RBCs to yield a mixture at 20% parasitemia. Polymersomes or nanomimics (both filled with fluorescent dye SRB) were then added to this mixture and incubated at 37 °C for 3 h under static conditions. After incubation, cells were fixed using 2% paraformaldehyde/0.2% glutaraldehyde in 0.1 M phosphate buffer (pH 7.4) at 4 °C overnight. Then, fixed samples were centrifuged at high speed (13.5 kRPM), redissolved in a small amount of PBS, and finally mounted on a slide using Vectashield supplemented with DAPI (Vector Laboratories).

Preparation of Parasites for TEM and 3D-SIM. For TEM and 3D-SIM imaging, merozoites were mechanically released from mature schizonts using a published protocol.[41] Briefly, 3D7 mature parasites were purified by Percoll density gradient and incubated with 10 μM E-64 inhibitor. After 6−8 h incubation, mature schizonts were filtered through 1.2 μm filters to release merozoites mechanically, immediately mixed with nanomimics, and incubated for 20 min at 37 °C. Then, merozoites were fixed in 2% paraformaldehyde/0.2% glutaraldehyde in 0.1 M phosphate buffer (pH 7.4) at 4 °C overnight. For TEM, samples were prepared according to Tokuyasu.[51] Briefly, merozoite−nanomimic complexes were washed in PBS and embedded in 12% gelatin, and thin blocks were infiltrated with 2.3 M sucrose overnight at 4 °C. Each centrifugation step was performed at high speed (13.5 kRPM). Ultrathin sections (80 to 100 nm) were prepared on an FC7/UC7-ultramicrotome (Leica) at −120 °C. For 3D-SIM fixed merozoites were collected by fast centrifugation (13.4 kRPM) and then mounted on a slide using Vectashield with DAPI as mounting medium.

Fluorescence Microscopy and Super-resolution 3D Structured Illumination Microscopy. Fluorescence micrographs were taken on a Leica DM 5000B fluorescence microscope. Image processing was performed on GIMP software.

3D-SIM was performed on a microscope system (DeltaVision OMX-Blaze version 4; Applied Precision, Issaquah, WA, USA) equipped with 405, 445, 488, 514, 568, and 642 nm solid-state lasers. Images were acquired using a Plan Apo N 60× 1.42 NA oil immersion objective lens (Olympus) and four liquid-cooled sCMOs cameras (pco Edge, full frame 2560 × 2160; Photometrics). Exciting light was directed through a movable optical grating to generate a fine-striped interference pattern on the sample plane. The pattern was shifted laterally through five phases and three angular rotations of 60° for each *z*-section. Optical *z*-sections were separated by 0.125 μm. The laser lines 405 and 568 nm were used for 3D-SIM acquisition. Exposure times were typically between 3 and 50 ms, and the power of each laser was adjusted to achieve optimal intensities of between 7000 and 10 000 counts in a raw image of 15-bit dynamic range at the lowest laser power possible to minimize photobleaching. Multichannel imaging was achieved through sequential acquisition of wavelengths by separate cameras.

Raw 3D-SIM images were processed and reconstructed using the DeltaVision OMX SoftWoRx software package (Applied Precision[52,53]). The resulting size of the reconstructed

images was 128 × 128 px from an initial set of 64 × 64 raw images. The channels were aligned in the image plane and around the optical axis using predetermined shifts as measured using a target lens and the SoftWoRx alignment tool. The channels were then carefully aligned using an alignment parameter from control measurements with 0.5 μm diameter multispectral fluorescent beads (Invitrogen, Molecular Probes)

Conflict of Interest: The authors declare the following competing financial interest(s): A patent application has been filed (EP14188354.6).

Supporting Information Available: Additional figures including reaction schemes, polymer characterization, TEM, DLS, SLS/DLS, Farndale microassays, FCS data, stopped-flow data, and cell toxicity. This material is available free of charge *via* the Internet at http://pubs.acs.org.

Acknowledgment. The Swiss National Science Foundation, NCCR Molecular Systems Engineering, and the University of Basel are acknowledged for financial support. The authors thank S. Kasper for PMOXA-*b*-PDMS-*b*-PMOXA synthesis, S. Lörcher for help with data analysis, J. T. Duskey for cell toxicity assays, P. Rigler for help with FCS, M. Lomora for help with stopped-flow measurements, S. Thamboo for help with sample preparation (all University of Basel), and S. Rusch for assistance with *Plasmodium* cultures (Swiss TPH). E. Angov (Division of Malaria Vaccine Development, Walter Reed Army Institute of Research, Silver Spring, MD, USA) is kindly acknowledged for providing *Pf*MSP1$_{42}$. We thank the Imaging Core Facility (IMCF, University of Basel) and in particular A. I. Ferrand for technical assistance provided on the OMX microscope. H. Stahlberg (C-CINA, University of Basel) is acknowledged for providing access to electron microscopes. B. A. Goodman is acknowledged for editing the manuscript, and T. Najer for designing the artistic illustration of the concept (Tobias Najer Grafikdesign + Illustration).

REFERENCES AND NOTES

1. Morens, D. M.; Folkers, G. K.; Fauci, A. S. The Challenge of Emerging and Re-emerging Infectious Diseases. *Nature* **2004**, *430*, 242–249.
2. Fauci, A. S.; Morens, D. M. The Perpetual Challenge of Infectious Diseases. *N. Engl. J. Med.* **2012**, *366*, 454–461.
3. Ashley, E. A.; Dhorda, M.; Fairhurst, R. M.; Amaratunga, C.; Lim, P.; Suon, S.; Sreng, S.; Anderson, J. M.; Mao, S.; Sam, B.; *et al*. Spread of Artemisinin Resistance in *Plasmodium falciparum* Malaria. *N. Engl. J. Med.* **2014**, *371*, 411–423.
4. Krachler, A. M.; Orth, K. Targeting the Bacteria-Host Interface: Strategies in Anti-Adhesion Therapy. *Virulence* **2013**, *4*, 284–294.
5. Bricarello, D. A.; Patel, M. A.; Parikh, A. N. Inhibiting Host−Pathogen Interactions Using Membrane-Based Nanostructures. *Trends Biotechnol.* **2012**, *30*, 323–330.
6. Bartlett, A. H.; Park, P. W. Heparan Sulfate Proteoglycans in Infection. In *Glycans in Diseases and Therapeutics*; Pavao, M. S. G., Ed.; Springer-Verlag: Berlin, 2011; pp 30−62.
7. World Health Organization. *World Health Statistics 2012*; World Health Organization: Geneva, 2012; pp 1−177.
8. McCormick, C. J.; Tuckwell, D. S.; Crisanti, A.; Humphries, M. J.; Hollingdale, M. R. Identification of Heparin as a Ligand for the a-Domain of *Plasmodium falciparum* Thrombospondin-Related Adhesion Protein. *Mol. Biochem. Parasitol.* **1999**, *100*, 111–124.
9. Boyle, M. J.; Richards, J. S.; Gilson, P. R.; Chai, W.; Beeson, J. G. Interactions with Heparin-like Molecules During Erythrocyte Invasion by *Plasmodium falciparum* Merozoites. *Blood* **2010**, *115*, 4559–4568.
10. Vogt, A. M.; Barragan, A.; Chen, Q.; Kironde, F.; Spillmann, D.; Wahlgren, M. Heparan Sulfate on Endothelial Cells Mediates the Binding of *Plasmodium falciparum*-Infected Erythrocytes via the DBL1alpha Domain of PfEMP1. *Blood* **2003**, *101*, 2405–2411.
11. Vogt, A. M.; Pettersson, F.; Moll, K.; Jonsson, C.; Normark, J.; Ribacke, U.; Egwang, T. G.; Ekre, H.-P.; Spillmann, D.; Chen, Q. Release of Sequestered Malaria Parasites Upon Injection of a Glycosaminoglycan. *PLoS Pathog.* **2006**, *2*, 853–863.
12. Adams, Y.; Freeman, C.; Schwartz-Albiez, R.; Ferro, V.; Parish, C. R.; Andrews, K. T. Inhibition of Plasmodium Falciparum Growth in Vitro and Adhesion to Chondroitin-4-Sulfate by the Heparan Sulfate Mimetic PI-88 and Other Sulfated Oligosaccharides. *Antimicrob. Agents Chemother.* **2006**, *50*, 2850–2852.
13. Hirsh, J.; Anand, S. S.; Halperin, J. L.; Fuster, V. Guide to Anticoagulant Therapy: Heparin: a Statement for Healthcare Professionals From the American Heart Association. *Circulation* **2001**, *103*, 2994–3018.
14. Xiao, L.; Yang, C.; Patterson, P. S.; Udhayakumar, V.; Lal, A. A. Sulfated Polyanions Inhibit Invasion of Erythrocytes by Plasmodial Merozoites and Cytoadherence of Endothelial Cells to Parasitized Erythrocytes. *Infect. Immun.* **1996**, *64*, 1373–1378.
15. Doolan, D. L.; Dobano, C.; Baird, J. K. Acquired Immunity to Malaria. *Clin. Microbiol. Rev.* **2009**, *22*, 13–36.
16. Kappe, S. H. I.; Vaughan, A. M.; Boddey, J. A.; Cowman, A. F. That Was Then but This Is Now: Malaria Research in the Time of an Eradication Agenda. *Science* **2010**, *328*, 862–866.
17. Srinivasan, P.; Yasgar, A.; Luci, D. K.; Beatty, W. L.; Hu, X.; Andersen, J.; Narum, D. L.; Moch, J. K.; Sun, H.; Haynes, J. D.; *et al*. Disrupting Malaria Parasite AMA1-RON2 Interaction with a Small Molecule Prevents Erythrocyte Invasion. *Nat. Commun.* **2013**, *4*, 2261.
18. Richards, J. S.; Beeson, J. G. The Future for Blood-Stage Vaccines against Malaria. *Immunol. Cell Biol.* **2009**, *87*, 377–390.
19. The RTS,S Clinical Trials Partnership. A Phase 3 Trial of RTS, S/AS01 Malaria Vaccine in African Infants. *N. Engl. J. Med.* **2012**, *367*, 2284–2295.
20. Ewer, K. J.; O'Hara, G. A.; Duncan, C. J. A.; Collins, K. A.; Sheehy, S. H.; Reyes-Sandoval, A.; Goodman, A. L.; Edwards, N. J.; Elias, S. C.; Halstead, F. D.; *et al*. Protective CD8$^+$ T-Cell Immunity to Human Malaria Induced by Chimpanzee Adenovirus-MVA Immunisation. *Nat. Commun.* **2013**, *4*, 2836.
21. Couvreur, P.; Vauthier, C. Nanotechnology: Intelligent Design to Treat Complex Disease. *Pharm. Res.* **2006**, *23*, 1417–1450.
22. Look, M.; Bandyopadhyay, A.; Blum, J. S.; Fahmy, T. M. Application of Nanotechnologies for Improved Immune Response against Infectious Diseases in the Developing World. *Adv. Drug Deliver. Rev.* **2010**, *62*, 378–393.
23. Huh, A. J.; Kwon, Y. J. "Nanoantibiotics": a New Paradigm for Treating Infectious Diseases Using Nanomaterials in the Antibiotics Resistant Era. *J. Controlled Release* **2011**, *156*, 128–145.
24. Santos-Magalhães, N. S.; Mosqueira, V. C. F. Nanotechnology Applied to the Treatment of Malaria. *Adv. Drug Delivery Rev.* **2010**, *62*, 560–575.
25. Discher, B. M.; Won, Y.-Y.; Ege, D. S.; Lee, J. C.; Bates, F. S.; Discher, D. E.; Hammer, D. A. Polymersomes: Tough Vesicles Made from Diblock Copolymers. *Science* **1999**, *284*, 1143–1146.
26. Lee, J. S.; Ankone, M.; Pieters, E.; Schiffelers, R. M.; Hennink, W. E.; Feijen, J. Circulation Kinetics and Biodistribution of Dual-Labeled Polymersomes with Modulated Surface Charge in Tumor-Bearing Mice: Comparison with Stealth Liposomes. *J. Controlled Release* **2011**, *155*, 282–288.
27. Najer, A.; Wu, D.; Vasquez, D.; Palivan, C. G.; Meier, W. Polymer Nanocompartments in Broad-Spectrum Medical Applications. *Nanomedicine (London, U.K.)* **2013**, *8*, 425–447.
28. Graff, A.; Sauer, M.; Van Gelder, P.; Meier, W. Virus-Assisted Loading of Polymer Nanocontainer. *Proc. Natl. Acad. Sci. U.S.A.* **2002**, *99*, 5064–5068.
29. Nazemi, A.; Haeryfar, S. M. M.; Gillies, E. R. Multifunctional Dendritic Sialopolymersomes as Potential Antiviral Agents: Their Lectin Binding and Drug Release Properties. *Langmuir* **2013**, *29*, 6420–6428.

30. Passirani, C.; Barratt, G.; Devissaguet, J.-P.; Labarre, D. Long-Circulating Nanoparticles Bearing Heparin or Dextran Covalently Bound to Poly Methyl Methacrylate. *Pharm. Res.* **1998**, *15*, 1046–1050.
31. Zhang, J.; Shin, M. C.; David, A. E.; Zhou, J.; Lee, K.; He, H.; Yang, V. C. Long-Circulating Heparin-Functionalized Magnetic Nanoparticles for Potential Application as a Protein Drug Delivery Platform. *Mol. Pharmaceutics* **2013**, *10*, 3892–3902.
32. Cowman, A. F.; Crabb, B. S. Invasion of Red Blood Cells by Malaria Parasites. *Cell* **2006**, *124*, 755–766.
33. Vogt, A. M.; Winter, G.; Wahlgren, M.; Spillmann, D. Heparan Sulphate Identified on Human Erythrocytes: a *Plasmodium Falciparum* Receptor. *Biochem. J.* **2004**, *381*, 593–597.
34. Nardin, C.; Hirt, T.; Leukel, J.; Meier, W. Polymerized ABA Triblock Copolymer Vesicles. *Langmuir* **2000**, *16*, 1035–1041.
35. Kumar, M.; Grzelakowski, M.; Zilles, J.; Clark, M.; Meier, W. Highly Permeable Polymeric Membranes Based on the Incorporation of the Functional Water Channel Protein Aquaporin Z. *Proc. Natl. Acad. Sci. U.S.A.* **2007**, *104*, 20719–20724.
36. Liu, J.; Pervin, A.; Gallo, C. M.; Desai, U. R.; Van Gorp, C. L.; Linhardt, R. J. New Approaches for the Preparation of Hydrophobic Heparin Derivatives. *J. Pharm. Sci.* **1994**, *83*, 1034–1039.
37. Sato, S.; Sakamoto, T.; Miyazawa, E.; Kikugawa, Y. One-Pot Reductive Amination of Aldehydes and Ketones with A-Picoline-Borane in Methanol, in Water, and in Neat Conditions. *Tetrahedron* **2004**, *60*, 7899–7906.
38. Stauch, O.; Schubert, R.; Savin, G.; Burchard, W. Structure of Artificial Cytoskeleton Containing Liposomes in Aqueous Solution Studied by Static and Dynamic Light Scattering. *Biomacromolecules* **2002**, *3*, 565–578.
39. Rigler, P.; Meier, W. Encapsulation of Fluorescent Molecules by Functionalized Polymeric Nanocontainers: Investigation by Confocal Fluorescence Imaging and Fluorescence Correlation Spectroscopy. *J. Am. Chem. Soc.* **2006**, *128*, 367–373.
40. Bacia, K.; Kim, S. A.; Schwille, P. Fluorescence Cross-Correlation Spectroscopy in Living Cells. *Nat. Methods* **2006**, *3*, 83–89.
41. Boyle, M. J.; Wilson, D. W.; Richards, J. S.; Riglar, D. T.; Tetteh, K. K.; Conway, D. J.; Ralph, S. A.; Baum, J.; Beeson, J. G. Isolation of Viable Plasmodium Falciparum Merozoites to Define Erythrocyte Invasion Events and Advance Vaccine and Drug Development. *Proc. Natl. Acad. Sci. U.S.A.* **2010**, *107*, 14378–14383.
42. Persson, K. E. M.; Lee, C. T.; Marsh, K.; Beeson, J. G. Development and Optimization of High-Throughput Methods to Measure *Plasmodium falciparum*-Specific Growth Inhibitory Antibodies. *J. Clin. Microbiol.* **2006**, *44*, 1665–1673.
43. Bijker, E. M.; Bastiaens, G. J.; Teirlinck, A. C.; van Gemert, G. J.; Graumans, W.; van de Vegte-Bolmer, M.; Siebelink-Stoter, R.; Arens, T.; Teelen, K.; Nahrendorf, W. Protection Against Malaria After Immunization by Chloroquine Prophylaxis and Sporozoites Is Mediated by Preerythrocytic Immunity. *Proc. Natl. Acad. Sci. U.S.A.* **2013**, *110*, 7862–7867.
44. Kita-Tokarczyk, K.; Grumelard, J.; Haefele, T.; Meier, W. Block Copolymer Vesicles—Using Concepts From Polymer Chemistry to Mimic Biomembranes. *Polymer* **2005**, *46*, 3540–3563.
45. Farndale, R. W.; Sayers, C. A.; Barrett, A. J. A Direct Spectrophotometric Microassay for Sulfated Glycosaminoglycans in Cartilage Cultures. *Connect. Tissue Res.* **1982**, *9*, 247–248.
46. Barbosa, I.; Garcia, S.; Barbier-Chassefière, V.; Caruelle, J.-P.; Martelly, I.; Papy-García, D. Improved and Simple Micro Assay for Sulfated Glycosaminoglycans Quantification in Biological Extracts and Its Use in Skin and Muscle Tissue Studies. *Glycobiology* **2003**, *13*, 647–653.
47. *Methods in Malaria Research*, 5th ed.; Moll, K.; Ljungström, I.; Perlmann, H.; Scherf, A.; Wahlgren, M., Eds.; MR4/ATCC: Manassas, VA, 2008; pp 673−675.
48. Dorn, A.; Stoffel, R.; Matile, H.; Bubendorf, A.; Ridley, R. G. Malarial Haemozoin/B-Haematin Supports Haem Polymerization in the Absence of Protein. *Nature* **1995**, *374*, 269–271.
49. Lambros, C.; Vanderberg, J. P. Synchronization of Plasmodium Falciparum Erythrocytic Stages in Culture. *J. Parasitol.* **1979**, *65*, 418–420.
50. Rivadeneira, E. M.; Wasserman, M.; Espinal, C. T. Separation and Concentration of Schizonts of Plasmodium Falciparum by Percoll Gradients. *J. Protozool.* **1983**, *30*, 367–370.
51. Tokuyasu, K. T. A Technique for Ultracryotomy of Cell Suspensions and Tissues. *J. Cell Biol.* **1973**, *57*, 551–565.
52. Gustafsson, M. G. Surpassing the Lateral Resolution Limit by a Factor of Two Using Structured Illumination Microscopy. *J. Microsc.* **2000**, *198*, 82–87.
53. Schermelleh, L.; Carlton, P. M.; Haase, S.; Shao, L.; Winoto, L.; Kner, P.; Burke, B.; Cardoso, M. C.; Agard, D. A.; Gustafsson, M. G. L.; *et al.* Subdiffraction Multicolor Imaging of the Nuclear Periphery with 3D Structured Illumination Microscopy. *Science* **2008**, *320*, 1332–1336.